Al-SiC IMPROVES RELIABILITY OF IGBT POWER MODULES

G. Lefranc [1], H.P. Degischer [2], K.H. Sommer [3], G. Mitic[1]

[1] *Siemens AG, Corporate Technology/Power Electronics, D-81730 Munich/Germany*
[2] *Vienna Univ. of Technology, Institute of Material Science & Testing, A-1040 Vienna/Austria*
[3] *eupec GmbH, D-59581 Warstein/Germany*

SUMMARY: Aluminium alloys reinforced by high volume fractions of SiC particulates are candidate materials for base plates of high power electronic modules. Such Al-SiC metal matrix composites exhibit low thermal expansion and high thermal conductivity similar to Cu-Mo alloys. The thermal expansion has to be matched to the ceramic substrate within the electronic package and has to be homogeneous over the plate to avoid degradation by thermally induced stresses. Three differently produced AlSiC base plates are investigated with respect to quality criteria like uniformity in micro-structure, as well as thermal and mechanical properties. The SiC volume fractions vary between 60 and 73% revealing different particle distributions. The linear coefficient of thermal expansion is decreasing with increasing SiC content from 7,9 to 6,5 ppm/K between room temperature and 150°C. The thermal conductivity, the Young's modulus and the elastic limit increase with increasing SiC volume fraction. The bending strength is related to the ductility.

KEYWORDS: SiC-particulate reinforced Al, Al-matrix, electronic packaging, insulated gate bipolar transistor, thermal properties, mechanical properties, micro-structure.

INTRODUCTION

With increasing concentration of energy dissipation in electronic components heat conduction becomes a decisive design criterion for high power electronic modules like IGBT (**I**nsulated **G**ate **B**ipolar **T**ransistor) modules [1,2]. Fig.1 illustrates the packaging of such an electronic module. The metal coated ceramic substrate is soldered on one side to the Si based chips and on the other side to the base plate, which is cooled. Fig.2 correlates the linear coefficients of thermal expansion to the lay up of materials. The changes in ambient temperature and moreover the heating during service causes thermally induced stresses between the different materials owing to their different coefficient of thermal expansion. Damage of the soft solder layer is enhanced by temperature cycles causing thermal fatigue of the solder joint due to crack propagation, which reduces the heat transfer and thus the electric efficiency and service life time of the module. Thermally matching, conductive material can be achieved by Al matrix composites containing high volume fractions of SiC particles [3,4]. The low thermal expansion of the ceramic constituent reduces that of the Al matrix according to the volume fraction and geometric arrangement within the composite. The reliability of the package will be increased essentially by approaching the thermal expansion of the substrate.

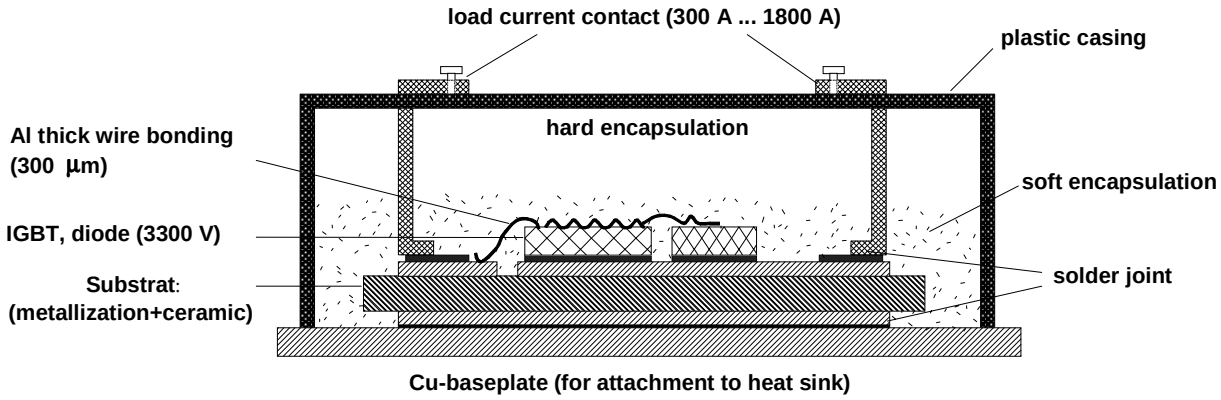

Fig.1: The design of IGBT power modules and the main functions of the components

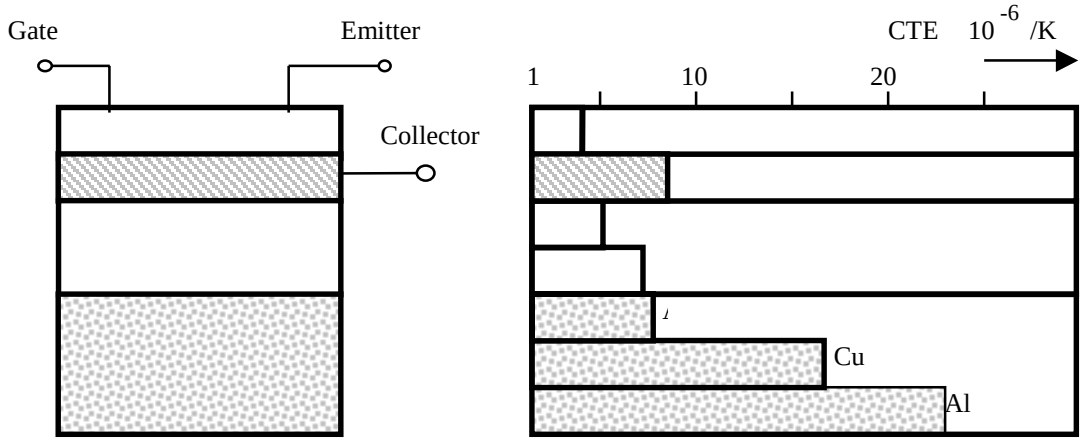

Fig.2: The lay up of an IGBT package and the CTE of corresponding material choices.

MATERIAL INVESTIGATED

The processing of AlSiC composites has to overcome the non wettability of molten aluminium towards ceramics by chemical driving forces or by external pressure [5]. Ceramic preforms of more than 40 vol.% SiC particulates can be prepared by ceramic green bond forming methods [6] and then infiltrated by the molten matrix. The Al-matrix has to be alloyed with Si to prevent extensive formation of Al-carbides at the interfaces to SiC. Three differently processed [7] prototypes of AlSiC base plates have been investigated: (1) = produced by reactive infiltration, (2) and (3) = by gas pressure infiltration of SiC particulate preforms.

CHARACTERISATION AND TESTING

The local distribution and volume fraction of the SiC particulates was investigated by light microscopy on polished cross sections of the plates parallel and perpendicular to their plane. Quantitative image analysis was applied to images of different magnifications to determine the size distribution of the particulates. The volume fraction of particulates was determined from optical micrographs representing areas of about 0,1 mm² each, which gives the local scatter of the particles content. At the same time any microstructural feature in the dimension of µm could be detected in the micrographs.

The coefficient of linear thermal expansion (CTE) was determined by dilatometric measurements in the temperature range between room temperature and 300°C [8]: the technical $CTE_t(\Delta T)$ is related to the length at starting temperature and is accurate to ±4%; the physical or instantaneous $CTE_p(T)$ is calculated within the interval T±10K yielding an accuracy of ±0,4 ppm/K. The thermal conductivity was determined by the thermal wave method and the heat capacity was measured in the temperature range of –55°C to +200°C by differential scanning micro-calorimetry with an accuracy of ±0,02 [J/g.K] [9,10]. The mechanical properties were investigated by four point bend tests at room temperature [11]. The force – deflection relations were transformed into stress – strain curves to deduce the elastic modulus, an elastic limit, the flexural strength and the elongation at rupture.

RESULTS

Table 1: Material properties and micro-structural features of the investigated AlSiC

No.	CTE [ppm]		H.Cap.	T.Cond.	4-Point Bend Test			SiC Particle Distribution				Defects
	50°C	RT-150°C	$C_p(T)$ [J/g.K]	λ [W/mK]	E [GPa]	R_b [MPa]	A [%]	total vol.%	small [µm]	med. [µm]	large (portion)	[vol.%]
(1)	7,3 ±0,3	7,9 ±0,3	RT 0,95	180	185 ±5	240 ±15	>0,5	61 ±3	1-5	7-10	15-35 (2/3)	<1 % porosity
(2)	6,8 ±0,3	7,4 ±0,2	–55°C 0,49 +100°C	185	190 ±6	390 ±25	>0,8	66 ±3	2-5	--	20-50 (3/4)	0,5 % SiC with impurities
(3)	5,7 ±0,8	6,5 ±0,2	0,70 +200°C 0,89	210	204 ±6	280 ±15	>0,5	73 ±4	1-4	6-9	30-80 (1/3)	4% particle free zones of ∅ 40-400 µm

Micro-Structure

The metallographic investigations revealed that the samples contain different size classes of SiC particulates. Light optical micrographs of typical particle distributions in different cross sections of the investigated materials are shown in Fig.3, where some defects are shown as well. Type (2) contains a bimodal size distribution whereas type (1) and (3) incorporate a third group of medium sized particles as well. Table 1 gives the size ranges of the SiC-particulates and the volume fractions averaged over local measurements by quantitative image analysis. The indicated portion of large SiC-particulates refers to the total volume fraction of all SiC-particulates. The irregularly shaped SiC particles exhibit an ellipsoidal ratio of their orthogonal dimensions. They are statistically oriented in type (3), but the bigger ones are preferentially oriented parallel to the plane of the type (1) and (2) plates as can be deduced from projected diameters determined by image analysis.

In Table 1, there are some defects quoted as well: In type (1) there is some porosity and the matrix concentration varies locally. In type (2) there are some particulates (bright in optical micrographs), which are SiC-particles containing V and Ti impurities. In type (3) there are spherical regions free of SiC particles of 0,04 to 0,4 mm in diameter as shown in Fig.3c. The distribution of SiC particulates was the same over the whole sample of each material, there are no gradients neither along the plates nor across their thickness.

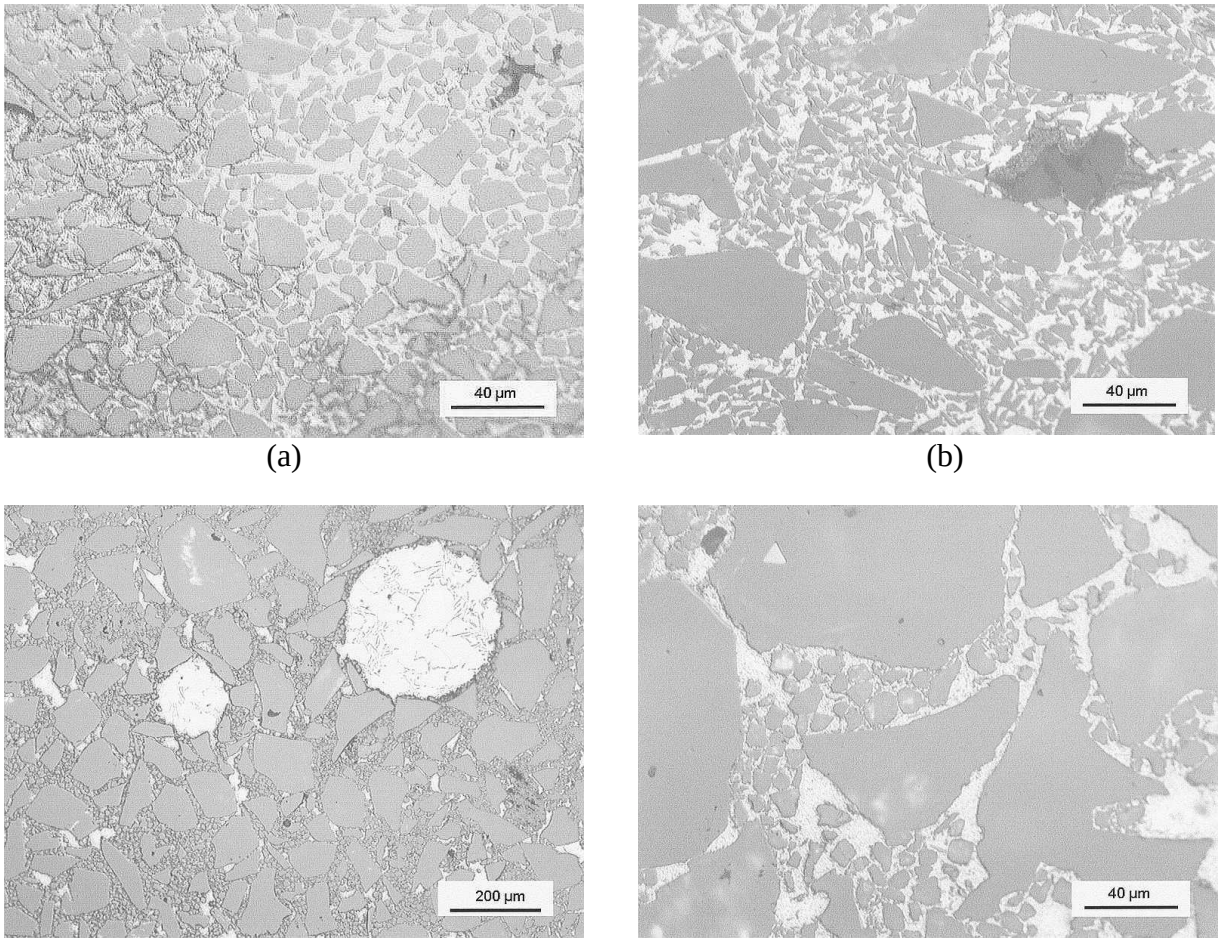

Fig.3: Optical micrographs of cross sections of investigated AlSiC-plates showing the particle distributions: (a) material (1) indicating inhomogeneity in the matrix and uninfiltrated pores; (b) material (2) with an impurity particle; (c) material (3) with typical particle free zone and (d) micrograph of material (3)in the same magnification as (a) and (b).

Thermomechanical Properties

Fig.4 shows the curves of linear thermal expansion for various heating and cooling cycles of the three types of materials. There is a slight elongation of type (2) and a pronounced elongation of type (3) observed after the first cycle. The instantaneous (physical), linear thermal expansion coefficient obtained by differentiation of the heating and cooling curves is plotted in Fig.5: CTE_p of the first and the third temperature cycles are plotted to indicate the range of data measured. The scatter for CTE_p of type (1) is relatively narrow within 1 ppm/K and the plots for type (2) are not shown as they are almost the same. The scatter of CTE_p of type (3) is wider and the CTE_p of the first heating is steadily increasing in contrast to the others. The physical CTE_p for 50°C (determined in the range ±10K) is listed in Table 1 with the scatter owing to all heating and cooling cycles.

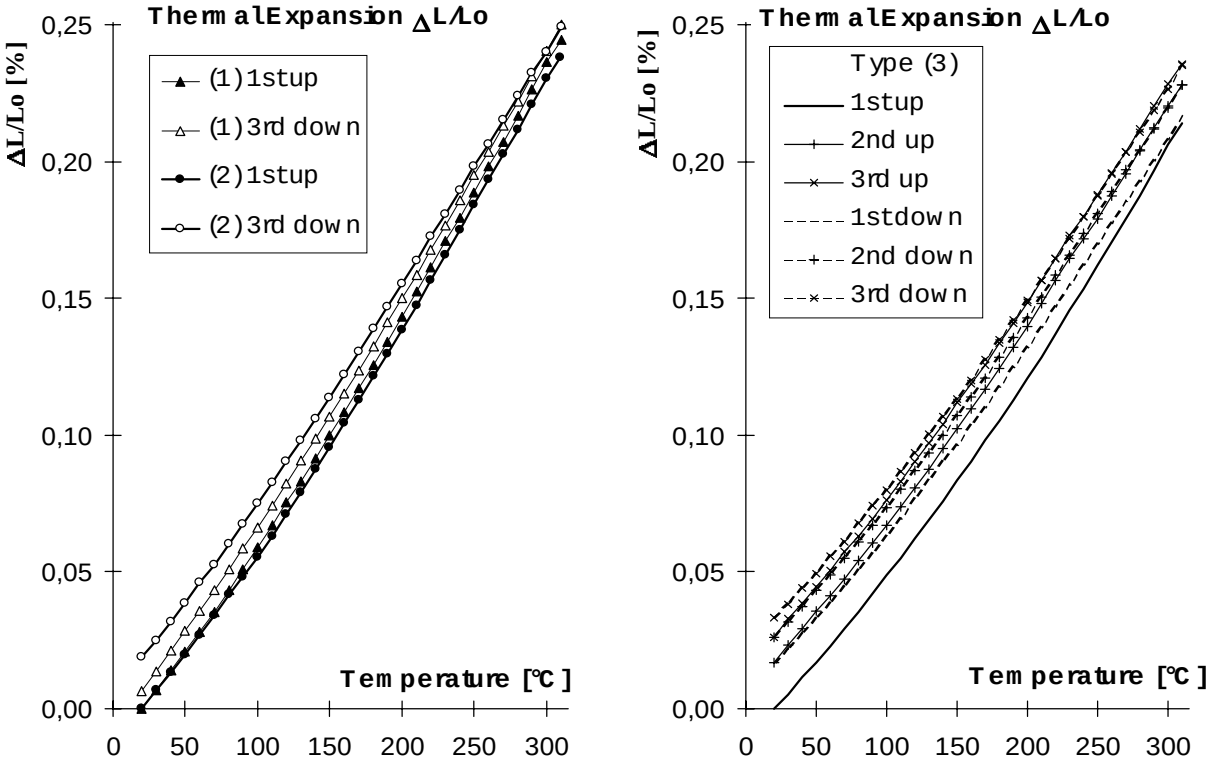

Fig.4: Dilatometer curves comparing the 1st and the 3ra heating cycle of materials (1) and (2) with 3 cycles of material (3), which exhibits a decreasing plastic expansion after each cycle

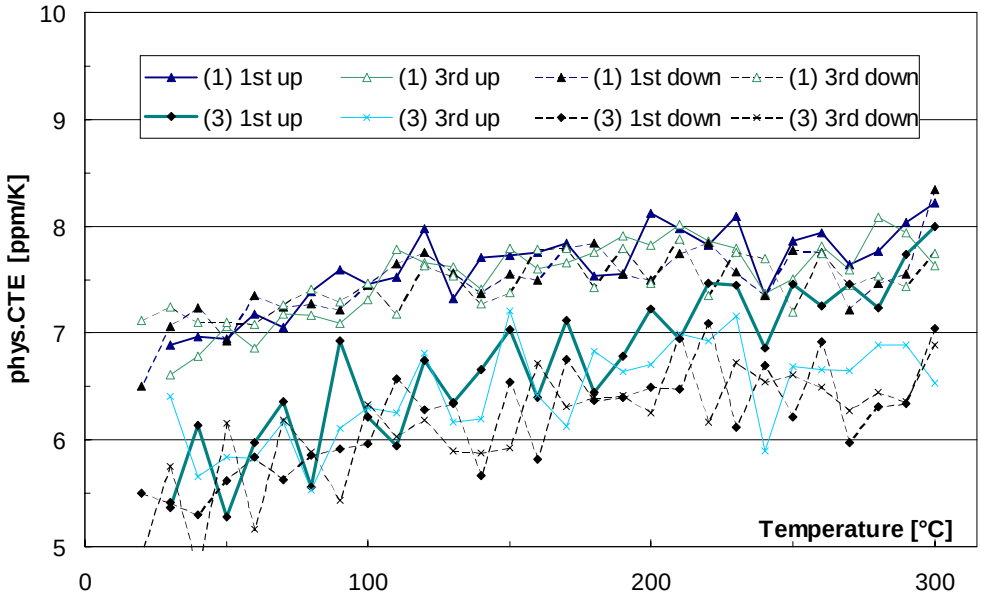

Fig.5: Representative dependence of the physical (instaneous), linear coefficients of thermal expansion of type (1) and (3) material on the thermal cycles. Note the steady increase of CTE_p of type (3) during the first heating.

The technical, thermal expansion coefficients from room temperature to 150°C are given as well in Table 1. The temperature dependence of the technical CTE_t referring to room temperature are plotted for the first heating of all types and for the first and third temperature cycle of type (3) in Fig.6. The CTE_t of type (1) and (2) are reproducible for all cycles, only type (3) depends on the cycle's number.

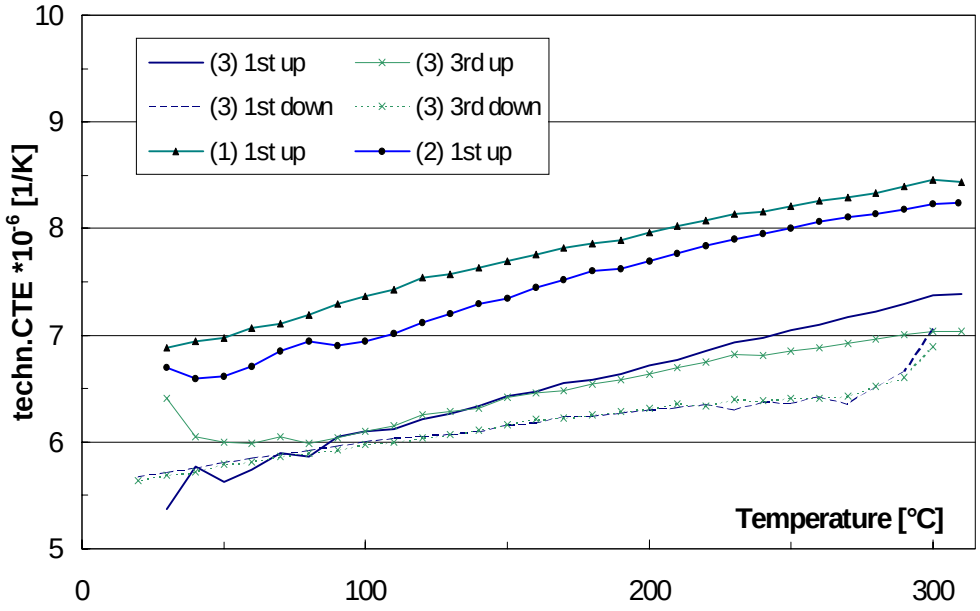

Fig.6: The temperature dependence of the technical, linear coefficient of thermal expansion for the 3 types of materials, of which CTE_t only for type (3) varies with the cycle's number.

The heat capacity is the same within the experimental accuracy for the type (2) and (3) materials tested. It is given for -55°C, +100°C and +200°C in Table 1. Type (1) material yields a significant higher value, which was measured only at room temperature.

Mechanical Properties

The stress - deflection curves of the 4-point bending tests show a clear linear range, of which the Young's modulus was determined as given in Table 1. The elastic limit for the matrix was defined at a plastic strain of 0,005% on the surface of the bending sample and denominated by $R_{p0,005}$: type (1) 100 MPa, type (2) 140 MPa, type (3) 170 MPa. The bending strength values and the corresponding elongation at rupture of the strained surface are given in Table 1. The values of the elongation at rupture scatter within 0,1% strain. The flexural strength increases with the ductility of the material as can be seen in Table 1: Type (2) has about 50% higher flexural strength (and elongation at rupture) than the other two materials.

CONCLUSIONS

The high volume fractions of SiC (>60 vol.%) are achieved already by bimodal particle size distributions. The function of the third, medium sized class in type (1) and (3) may be questioned. The preforms of type (1) and (2) had been mechanically compressed to form plates, which yields the observed planar orientation of the large, slightly elongated SiC-particles. In type (3) even elongated particles are statistically oriented, because those preforms had been prepared without compression. The distribution of particles across the samples is statistically homogeneous, except for the "bubbles" in the preforms of type (3), which are filled just with matrix. These "bubbles" may cause local deformations of the plates by thermal stresses, where they touch the surface. The chemically driven infiltration of type (1) material results in a slightly inhomogeneous structure, which exhibits some local accumulations of pores and fluctuations in the chemical concentration of the matrix.

The impurities in a few of the SiC-particles in type (2) should not affect the properties significantly. Although with increasing purity of SiC the thermal conductivity increases reaching more than 200 W/mK [5], which is higher than that of the matrix alloy of about 180 W/mK. The thermal conductivity of AlSiC as given in Table 1 increases with the SiC content.

Generally the CTE of all investigated AlSiC materials is close to that of alumina (see Table 2 [12]) and decreases with increasing particle content as shown in Fig.7 approximately according to a linear rule of mixture [13]. The remarkable plastic elongation of the samples of type (3) during the first heating indicates that the material originally contains internal stresses, which relax during heating by plastification of the matrix. The following slow cooling rate in the dilatometer does not restore these stresses, therefore further thermal cycles yield a reversible elongation. Type (1) and (2) materials were either slowly cooled after infiltration or after a following annealing treatment. A higher yield strength of the matrix may contribute as well to enhanced internal stresses. The decrease in yield strength of the matrix with increasing temperature causes the physical CTE_p to approach a constant value for all thermal cycles of type (1) above 150°C and of type (2) above 180°C, but as well for the 2nd and 3rd cycle of type (3) above 200°C (see Fig.5). The difference in matrix strength is confirmed by the bending strength, which increases in the same order. Although the yield strength is plotted versus the SiC volume fraction in Fig.8, this should not be interpreted as an exclusive causal correlation.

Table 2: Comparison of properties of pure metals, ceramic substrate, packaging materials.

Properties	Units	Cu	Al	Al_2O_3	AlN	AlSiC	CuMo15
Density	g/cm³	8,9	2.7	3,8	3,3	3	10
CTE_t (150°C)	ppm/K	17	23	6,7	4,5	7	6,5
Therm.Cond.	W/mK	350	220	27	190	200	180
E-Modulus	GPa	125	70	390	340	200	300
Strength	MPa	300	150	R_b: 440	R_b: 400	R_b: 300	800

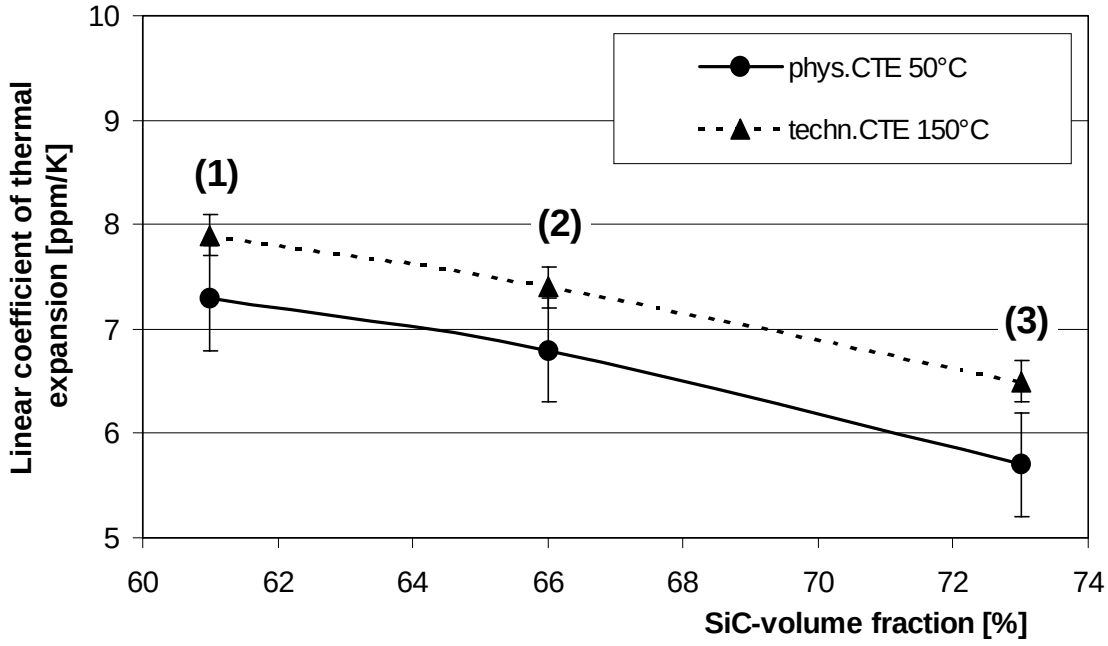

Fig.7: Physical and technical linear coefficient of thermal expansion of the 3 types of AlSiC correlated to the volume fraction of SiC-particles.

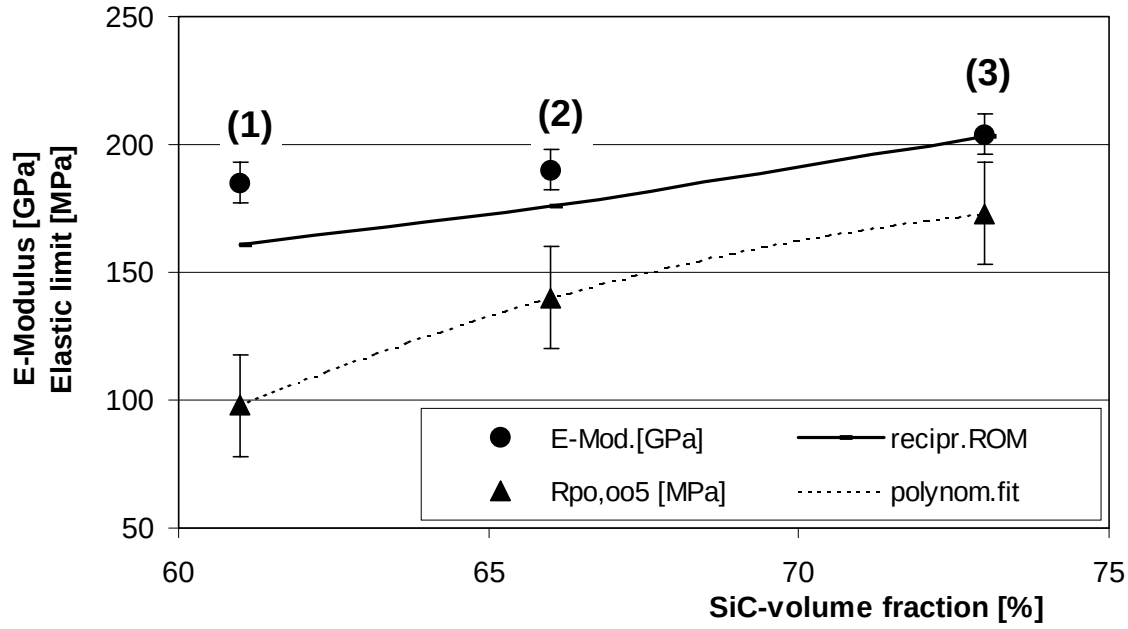

Fig.8: The Young's moduli related to the volume fraction of SiC-particles compared with the reciprocal rule of mixture (ROM) and the $R_{p0,005}$ yield strength of the 3 types of AlSiC

The increase of the Young's modulus with the SiC content can be predicted by the reciprocal rule of mixtures [13], but as Fig.8 shows, the measured values for type (1) and (2) are rather above the theoretical ones assuming E_{matrix} = 78 GPa (highly alloyed matrix) and E_{SiC} = 550 GPa (high quality SiC [14]), which can be attributed to the planar orientation of the big SiC-particles.

The mechanical and physical properties of the tested AlSiC materials are appropriate for applications as base plate of IGBT modules and as material for heat sink. The thermal conductivity is even higher than that of CuMo15. A rather soft matrix and an annealing treatment is recommended for AlSiC to reduce internal stresses. The defects as observed in type (1) and (3) material should be eliminated to improve the uniformity in performance. The reliability of devices for high power modules is usually tested by thermal cycling between -55°C and 150 °C, where slight distortions could be observed causing thermal fatigue of the solder, which is to be reduced to avoid delamination. It is required that the original material properties are preserved after this test.

ACKNOWLEDGEMENTS

This work has been partially supported by the German 'Bundesministerium für Bildung, Wissenschaft, Forschung und Technologie' under contract 16SV821/1

REFERENCES

[1] Hierholzer, M., “Application of high power IGBT Modules”, Proc. PCIM 96, 1996, 26.

[2] Sommer, K. H. et al., “Multichip high power IGBT-Modules for traction and industrial application”, Proc. EPE97, 1997

[3] Zweben, C., “Metal Matrix Composites for Electronic Packaging”, JOM, 1992, pp.15-23.

[4] Premkumar, M.K., Hunt, W.H., Sawtell, R.R., “Aluminium Composite Materials for Multichip Modules”, JOM, 1992, pp.24-26.

[5] Suresh, S., Mortensen, A., Needleman, A., “Fundamentals of Metal Matrix Composites”, Butterworth-Heinemann, Stoneham/MA, 1993.

[6] Kolaska, H., “Pulvertechnologische Wege in die Zukunft”, DGM, Oberursel 1995.

[7] Asthana, R., “Solidification Processing of Reinforced Metals”, Trans Tech Publ., Zürich, 1998.

[8] Heß, R., ARCS Internal Report, Seibersdorf, 1998.

[9] Beyfuss, M. et al., “Thermal characterization of thin layers”, in Photoacoustic and Photothermal Phenomena III, Vol. 69, Springer, 1992.

[10] Muschik, H. TGM-Prüfbericht K17520 according to DIN 53 765, Wien, 1998.

[11] Schulz, P., ARCS-LKR Prüfbericht according to DIN 51 110, Ranshofen, 1998.

[12] Lostetter, A. et al., “Thermal evaluation and comparison study of power baseplate materials”, in Advancing Microelectronics, 1998, Vol. 25, No. 1, pp. 25-27.

[13] Clyne, T.W., Withers, P.J., “An Introduction to Metal Matrix Composites”, Cambridge Univ.Press, 1993.

[14] Bloor, D. et al., “The Encyclopedia of Advanced Materials”, Vol.4, Pergamon, Cambridge/MA, 1994.